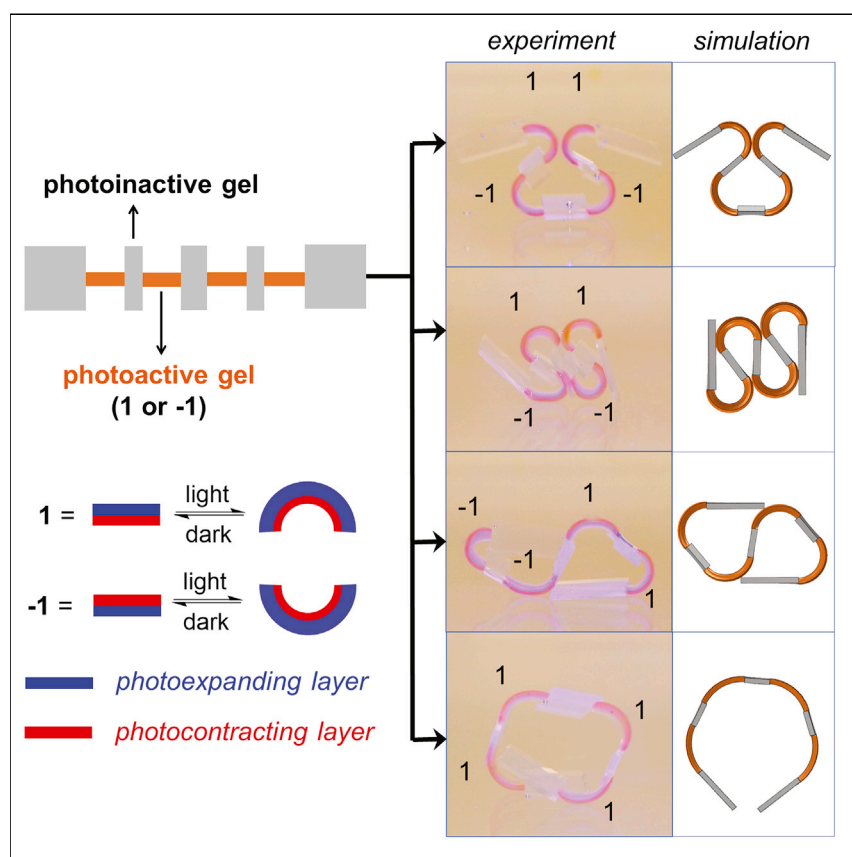


Article

Synergistic photoactuation of bilayered spiropyran hydrogels for predictable origami-like shape change



Bilayered hydrogels were designed using spiropyran molecular photoswitches with opposite volumetric change response to visible light. The coupling of expanding and contracting layers was found to generate synergistic bending actuation in response to light. Constructs with specific sequences of bilayered and photoinactive hydrogels also undergo origami-like 3D shape transformations. Bio-inspired unidirectional locomotion of the constructs on surfaces was also observed in patterned hydrogels exposed to periods of light and darkness. Analytical modeling predicts the observed shape changes and locomotion.

Chuang Li, Yeguang Xue,
Mengdi Han, Liam C. Palmer,
John A. Rogers, Yonggang
Huang, Samuel I. Stupp

y-huang@northwestern.edu (Y.H.)
s-stupp@northwestern.edu (S.I.S.)

HIGHLIGHTS

Bilayer hydrogels exhibit opposite volumetric change in response to light exposure

Coupling expanding and contracting layers generates synergistic bending with light

Constructs exhibit light-driven locomotion and origami-like 3D shape changes

Observed shape changes in designed constructs predicted by analytical modeling



Demonstrate

Proof-of-concept of performance with intended application/response

Li et al., Matter 4, 1377–1390

April 7, 2021 © 2021 Elsevier Inc.

<https://doi.org/10.1016/j.matt.2021.01.016>



Article

Synergistic photoactuation of bilayered spiropyran hydrogels for predictable origami-like shape change

Chuang Li,^{1,10} Yeguang Xue,^{2,3,4,10} Mengdi Han,⁵ Liam C. Palmer,^{1,6,9} John A. Rogers,^{1,2,3,5,6,7,9} Yonggang Huang,^{2,3,4,5,*} and Samuel I. Stupp^{1,2,6,7,8,9,11,*}

SUMMARY

Development of stimuli-responsive soft matter that undergoes fast and reversible shape changes that mimic living organisms is a grand challenge for materials science. We report here on the molecular design of photoactive bilayer actuators that can rapidly respond to visible light, leading to complex but predictable bio-inspired shape changes. The mechanism of accelerated actuation is rooted in the simultaneous photoexpansion of one layer and photocontraction of the other triggered by the same light stimulus. The opposing response leads to a synergistic effect that results in fast bending actuation. The synergistic bilayers were bridged with light-inactive segments to generate macroscopic constructs capable of undergoing programmable 3D origami-like shape change upon irradiation. By controlling the anisotropic friction with the substrate, these constructs displayed unidirectional inchworm- and octopus-like locomotion over macroscopic distances. The soft matter systems investigated here demonstrate the possibility of molecularly engineering photoactuators that mimic functions we associate with living organisms.

INTRODUCTION

Bilayered or multilayered structures are widespread across a broad range of plant and animal tissues and their architectures contribute to their complex biological functions. For example, the anisotropic layers of cellulose fibrils in plants induce hygroscopic actuation in response to humidity and govern the opening and closing of pine cones,¹ direct the pumping movements of wheat awns that propel seeds to the ground,² and trigger the reversible origami-like folding and unfolding of ice plant seedpods.³ Inspired by these natural systems, layered synthetic materials and devices across different length scales have been developed for mechanical actuation applications. By combining a layer of an actuating material with a “passive” non-actuating component, it is possible to achieve an anisotropic deformation rather than the isotropic expansion or contraction expected for the actuating component alone. This effect has been demonstrated using many different bilayered or multilayered materials with components such as solid polymer films,^{4–8} liquid crystal elastomers,^{9,10} and hydrogels.^{11–14} Hydrogels are unique soft matter for such actuation applications due to their hydrated nature and ability to change volume by absorbing or expelling water.^{15,16} Two particularly noteworthy examples include 4D-printed cellulose-based bilayer architectures that change shape upon immersion in water¹⁷ and gel structures photopatterned with multiple domains that allow localized actuation in response to DNA sequences complementary to those domains.¹⁸ Bilayer

Progress and potential

A grand challenge for materials science is the development of biomimetic soft matter that emulates behaviors of living creatures in response to an energy input. Photoresponsive hydrogels are particularly attractive in this context because they can expand or contract in response to light through reversible changes in molecular structure and internal water content. Using hydrogels developed recently in our laboratory, which expand with light exposure, and previously known ones that contract, we report here on the synergistic faster bending actuation of bilayered hydrogels with opposite response to light. We also show that constructs with chemically connected sequences of bilayer and photoinactive hydrogels undergo reversible and predictable origami-like 3D shape changes as well as unidirectional walking motion when exposed to light and dark periods. This work advances our ability to design molecularly life-like behavior in robotic soft materials responding to external stimuli.



hydrogels have also been reported in which the two layers have components that are both stimuli responsive, leading to bending in one direction or the other depending on the stimulus.^{13,19–22}

Light is a particularly useful stimulus since it does not require physical contact with materials and also because of the versatility offered by wavelength and intensity tunability.^{23–27} This versatility can be used in photoresponsive materials, such as liquid crystal networks (LCNs)²⁸ and hydrogels,^{29–32} functionalized with molecular photoswitches.^{33–35} In these systems, conformational changes as a result of photoisomerization can lead to the macroscopic shape changes in hydrogels.^{36–39} For example, photocontraction of hydrogels through the isomerization of protonated merocyanine (MCH⁺) to spiropyran (SP) moieties^{40,41} is a well-known phenomenon.^{42–45} In recent work we reported on the synthesis of water-soluble spiropyran structures covalently embedded in a 3D hydrogel network that led to photoexpansion of hydrogels.⁴⁶ Previously reported examples of deformation and actuation are based on photoisomerization gradients, but layered spiropyran-based materials have not been reported. Using a combination of both photocontracting and photoexpanding layers that are simultaneously responsive to a single light stimulus, we report here on the design of synergistic bilayer photoactuators and investigate their unique photoactuation behavior.

RESULTS AND DISCUSSION

Design and preparation of synergistic bilayer photoactuators

Here, we prepared a series of bilayer structures in which individual layers expand, contract, or remain unresponsive to light. The photoexpanding layer is composed of a poly(*N*-isopropylacrylamide) (PNIPAM) backbone grafted with a water-soluble spiropyran moiety bearing two negatively charged sulfonate substituents (SP₁). Photoisomerization of the protonated merocyanine (MCH⁺) to the spiropyran (SP²⁻) form caused an increase in net charge density, resulting in hydrogels that absorb water molecules thus expanding to 130% of their original dimension (Figure 1A). On the other hand, the photocontracting layer contains the same PNIPAM backbone with a different hydrophobic spiropyran moiety (SP₂) that has a similar absorbance spectrum (Figure S1A) and a comparable photoisomerization rate (Figure S1B). The resulting photocontracting material displayed similar mechanical properties (Figure S2) to the photoexpanding layer. Upon irradiation with the same light, it isomerizes from the MCH⁺ to the SP form and the decrease in net charge density drives the hydrogel to expel water and contract to 83% of its initial volume (Figure 1B). Photoinactive layers without spiropyran moieties were used here as the light-unresponsive layers (Figure 1C). A two-step free radical polymerization procedure was used to glue each individual layer to obtain four different bilayer objects in total (each 10 mm long, 2 mm wide, and containing two 0.3 mm layers, see the [Experimental procedures](#) and [Supplemental information](#) for details), namely *exp-con* (expansion-contraction), *exp-bl* (expansion-blank), *bl-con* (blank-contraction), and *bl-bl* (blank-blank, bottom layer-top layer). We fabricated the bilayers by partially polymerizing the first layer followed by addition of the second set of precursors and initiating polymerization of the second layer to ensure chemical linking of the two layers, which is critical for their structural stability as actuators. Cross-sectional scanning electron microscopy of these bilayer samples revealed that they are tightly adhered to each other at their interface (Figure S3). Confocal laser scanning microscopy also confirmed the adhesion of the two bonded layers (Figure S4). These four bilayer objects were found to display different photoactuation behavior under the same light illumination because objects containing photoactive layers bend up, while the

¹Center for Bio-inspired Energy Science, Northwestern University, Evanston, IL 60208, USA

²Department of Materials Science and Engineering, Northwestern University, Evanston, IL 60208, USA

³Department of Mechanical Engineering, Northwestern University, Evanston, IL 60208, USA

⁴Department of Civil and Environmental Engineering, Northwestern University, Evanston, IL 60208, USA

⁵Center for Bio-Integrated Electronics, Northwestern University, Evanston, IL 60208, USA

⁶Department of Chemistry, Northwestern University, Evanston, IL 60208, USA

⁷Department of Biomedical Engineering, Northwestern University, Evanston, IL 60208, USA

⁸Department of Medicine, Northwestern University, Chicago, IL 60611, USA

⁹Simpson Querrey Institute, Northwestern University, Chicago, IL 60611, USA

¹⁰These authors contributed equally

¹¹Lead contact

*Correspondence:
y-huang@northwestern.edu (Y.H.),
s-stupp@northwestern.edu (S.I.S.)

<https://doi.org/10.1016/j.matt.2021.01.016>

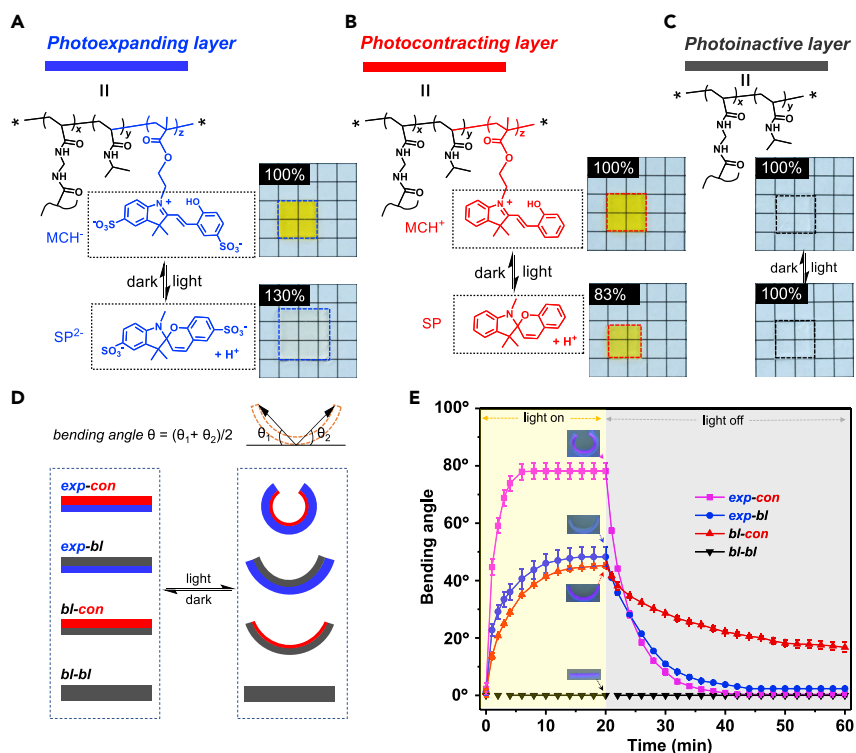


Figure 1. Design and preparation of synergistic bilayer photoactuators

(A) Molecular structure of the photoexpanding hydrogel containing a spiropyran moiety substituted by two sulfonate groups and photographs depicting the light-triggered expansion of the gel.

(B) Molecular structure of photocontracting hydrogel containing a spiropyran moiety and photographs of the light-triggered contraction of the gel.

(C) Molecular structure of the photoinactive hydrogel and photographs of the gel before and after irradiation.

(D) Schematic representation of four bilayer objects exhibiting different bending behaviors upon irradiation (the definition of bending angle is shown at the top; “exp” indicates “expansion”, “con” indicates “contraction”, and “bl” indicates “blank”).

(E) Plot of the bending angle of bilayer objects (each 10 mm long, 2 mm wide, and containing two 0.3 mm layers) versus time for one actuation cycle, including the light exposure (yellow) and dark (gray) periods (the insets are photographs of bilayer objects with maximum bending triggered by light). Error bars represent standard deviations of data collected from three separate samples.

photoinactive *bl-bl* bilayer keeps its flat geometry (Figure 1D). Interestingly, the synergistic *exp-con* bilayer object showed a larger bending angle (78°) relative to either the *exp-bl* (48°) or *bl-con* (45°) bilayers (Figure 1E; Video S1), indicating that the combination of expanding and contracting layers generates a greater deformation gradient responsible for the observed shape changes. In addition, synergistic bilayer objects create a faster bending speed (13°/min) by a factor of ~4–5 relative to that of either *exp-bl* (3°/min) or *bl-con* bilayers (2.8°/min). This acceleration was also observed during the relaxation process in the dark, when spiropyran moieties spontaneously switched back to the more thermally stable form of protonated merocyanine and the bending objects recovered to their original flat state. It was found that the relaxation time of synergistic *exp-con* bilayer was 15 min, whereas 20 min was required for relaxation of the *exp-bl* bilayers and 90 min for the *bl-con* bilayers. Video S2 shows the first 40 min of the recovery process of these three bilayers, but the *bl-con* bilayer actuator does not fully recover to its original flat shape within this period of time. The reason for the slow recovery of the *bl-con* bilayer might be

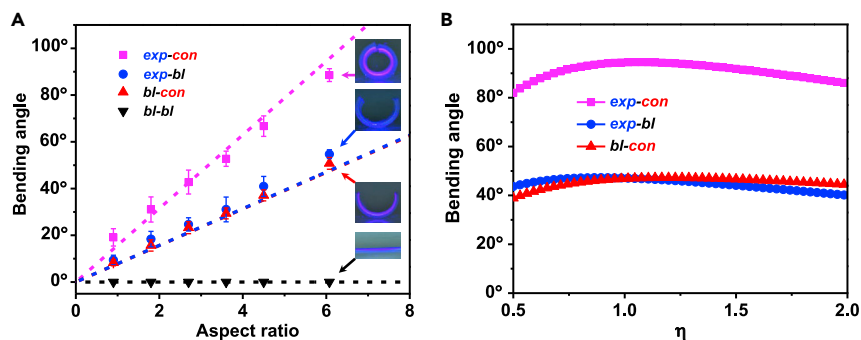


Figure 2. Tunable bending behaviors of synergistic bilayer photoactuators

(A) Plot of the maximum bending angle versus aspect ratio for four different bilayer objects with fixed thickness and width of 0.6 mm (0.3 + 0.3) and 2.0 mm, respectively. Dots are experimentally measured bending angles (error bars represent standard deviations of data collected from three separate samples) and the dashed lines are calculated from an analytical model (see the [Experimental procedures](#)).

(B) Plot of the bending angles calculated from the analytical model as a function of the ratio of the top layer thickness to that of the bottom layer (η) corresponding to three different bilayer objects with fixed length, width, and total thickness of 12.0, 2.0, and 0.6 mm, respectively.

that the contracting layer containing SP₂ becomes denser upon irradiation, which in turn slows water diffusion and recovery to its initial shape under dark conditions. By switching light on and off, these bilayer objects were able to bend and unbend for multiple cycles ([Figure S5](#)), demonstrating the high reversibility and robustness of this actuation system.

In addition to PNIPAM, we also prepared synergistic bilayer photoactuators using polyacrylamide (PAM), which is not thermally responsive. The original dimensions of the photoexpanding (PAM-SP₁) and photocontracting layers (PAM-SP₂) changed to 116% and 87% of their original dimensions upon light irradiation, respectively ([Figures S6A](#) and [S6B](#)). These volumetric changes, especially the photoexpansion ratio, were found to be smaller than those observed in PNIPAM-SP hydrogels, which is consistent with our previous finding that spiropyran-containing polymer hydrogels with a higher lower critical solution temperature (LCST) exhibit a lower photoexpanding ratio.⁴⁶ Because of the smaller volumetric change, the synergistic bilayer containing PAM was found to display a smaller bending angle and a slower bending rate compared with one containing PNIPAM under the same irradiation conditions ([Figures S6C](#) and [S6D](#)). These results offered us an additional strategy to tune the photoactuation performance of the synergistic bilayer actuators by simply changing polymer composition.

Photoactuation performance of synergistic bilayer actuators

The concept of synergistic bilayer photoactuation to enhance performance was also tested in hydrogel objects with different dimensions. [Figure 2A](#) shows that *exp-con* bilayer objects display larger bending angles with increasing aspect ratio (fixing thickness and width but increasing length) ([Figure S7](#)). This observation was in good agreement with the calculated results from the analytical model (linear dashed lines, see the [Experimental procedures](#) for details), which predicted the slope of this curve to be greater by a factor of ~ 2.0 for *exp-con* bilayer objects relative to that for *exp-bl* and *bl-con* bilayers. We investigated how the thickness of each layer affects the overall deformation behavior while keeping the aspect ratio at a fixed value. For this purpose, we define η as the thickness ratio between the top and bottom layers. As shown in [Figure 2B](#), the analytical model verified that the bending angle

of a bilayer with synergistic behavior (*exp-con*) tends to be larger than that of either the *exp-bl* or *bl-con* bilayers, indicating that the synergy is valid over different thickness ratios of the two layers. More importantly, all three curves are nearly flat, suggesting that the bending angle should be nearly independent of the relative thicknesses of the two layers (η) over the range 0.5–2.0. The slight increase at low values and minimal decline at high values of η indicated that the bending angle tends to be optimal when η is close to 1. Therefore, in subsequent experiments we used bilayer objects with a fixed η value of 1.0 and a fixed thickness of 0.3 mm for each layer. To gain more insight into the driving force generated during photoactuation, we calculated the bending moment that is required to flatten the bent bilayer using our analytical model (see the [Experimental procedures](#) for details). [Figure S8](#) shows that the model predicts the synergistic *exp-con* bilayer to have a nearly 2-fold greater bending moment (2.0×10^{-7} N·m) relative to that of the *exp-bl* and *bl-con* bilayers. We suggest this difference explains the enhanced actuation performance observed in the synergistic bilayer system.

Programmed origami-like shape changes

Based on its actuation performance, the synergistic *exp-con* bilayer was used to further design functional structures that are capable of programmable shape changes in response to light. We prepared rectangular bilayer constructs as photoactive units and define *exp-con* (bottom layer-top layer) units as -1 and the inverted unit *con-exp* as 1 ([Figure 3A](#)). After assembling these photoactive units (1 or -1) into a desired predetermined sequence, a solution containing NIPAM monomers was added and polymerized to join these photoactive units. A series of linear structures with specific sequences of photoactive and photoinactive units were prepared and are listed in [Figure 3B](#) (see the [Experimental procedures](#) and [Supplemental information](#) for details). The linear structures (*Lin-1* to *Lin-8*) contained a total of four photoactive units (i–iv) and maintained identical flat geometry in the dark ([Figure S9](#)). However, these flat objects exhibited clear 3D bending and folding behaviors upon irradiation with visible light (450 nm) ([Figure 3C](#); [Video S3](#)). These photo-induced origami-like shape changes were programmed by predetermined permutations of the four photoactive units. This programmability allows us to create light-activated shape transformations, which are predicted with finite element simulations by fitting the experimental parameters, such as moduli and expansion/contraction strain ([Figure 3C](#), bottom; see the [Experimental procedures](#) and [Supplemental information](#) for details). Following the same principle, we designed and prepared cross-shaped structures containing eight photoactive units with variable permutations of 1 and -1 that can transform into complex 3D geometries upon irradiation with visible light ([Video S4](#)). [Figure 3D](#) illustrates four different permutations as well as their corresponding 3D configurations from both experiments (top) and simulations (bottom). In addition, we designed a branched structure containing a total of 12 photoactive units that exhibited a more complex configuration upon irradiation with visible light ([Figure 3E](#); [Video S5](#)). The abrupt shape changes observed in [Videos S3](#), [S4](#), and [S5](#), are likely due to friction between the hydrogel actuator and the substrate. The hydrogel actuator requires a sufficient bending force to overcome the friction before an actual shape change can occur. This bending force originates from the light-induced gradient of expansion/contraction between the two layers, which is a slow process. If the bending force is smaller than the critical value needed to overcome the friction at a time point, then no shape change occurs. However, once the bending force exceeds this friction, the hydrogel object rapidly changes shape due to a rapid release of free energy. Importantly, all these shape transformations are highly reversible, as the bending structures gradually recover their original flat shapes in the dark due to spiropyran moieties switching back to the merocyanine structure.

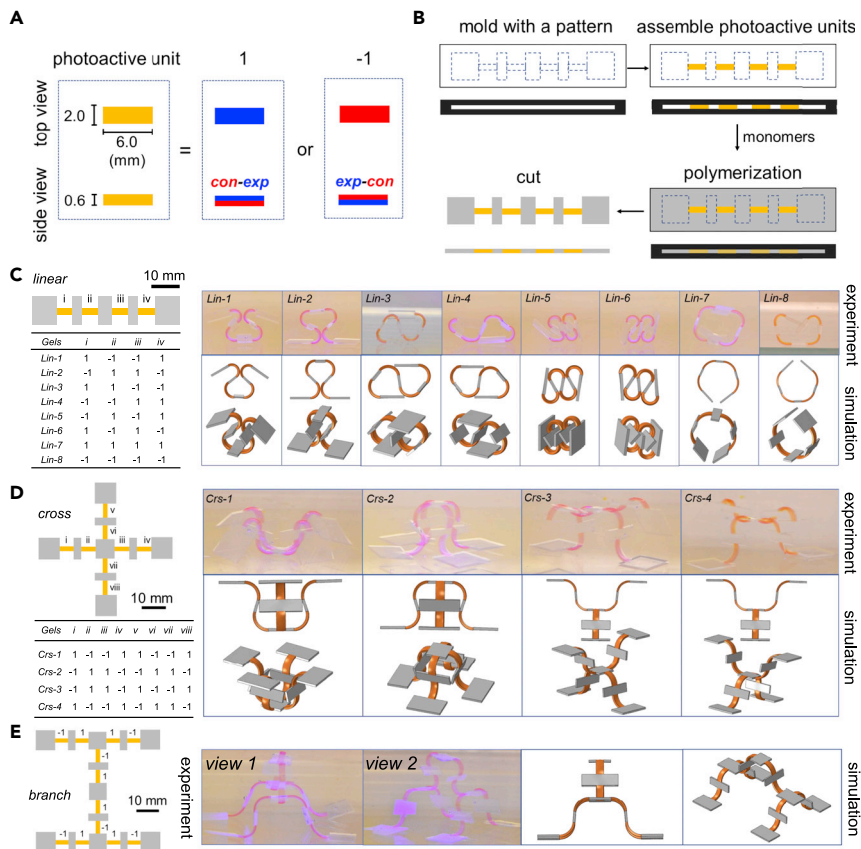


Figure 3. Programmable origami-like shape changes of macroscopic constructs triggered by light

(A) Dimensions and definition of photoactive units 1 and -1; the synergistic bilayer object con-exp is labeled 1 and its inverse exp-con as -1. To simplify, both photoactive units are shown in orange color hereafter.

(B) Preparation of linear block structures using photoactive units (1 or -1, orange) and photoinactive blank units (gray).

(C) Linear block structures containing four photoactive units with variable permutations of 1 and -1 undergo different shape transformations upon irradiation with visible light (450 nm); photographs of the deformation geometries observed in eight different sequences of photoactive and photoinactive units are shown at the top (*Lin-1* to *Lin-8*) with their corresponding snapshots from finite element simulations at the bottom.

(D) Cross-shaped objects containing eight photoactive units with variable permutations of 1 and -1 reveal distinct light-induced shape transformations; photographs of shapes from four different sequences (*Crs-1* to *Crs-4*) are shown at the top with their corresponding snapshots from finite element simulations at the bottom.

(E) Branch-shaped structures containing a total of 12 photoactive units that bend up upon irradiation; photographs of 3D configurations are shown on the left and corresponding snapshots from finite element simulations on the right.

Inchworm-like crawling motion of linear macroscopic constructs

To demonstrate potential robotic functions, such as locomotion of these shape-morphing objects, we built millimeter-scale ratcheted structures at the bottom of some of the photoinactive segments using a ratchet mold transfer method (see the [Experimental procedures](#) and [Supplemental information](#) for details). The hydrogel objects with these anisotropic ratchets exhibited anisotropic friction with the substrate they were in contact with during shape transformation, which in turn we found could be used to control their locomotion direction. [Figure 4A](#) illustrates two types of inchworm-like walkers (code (-1)11(-1) for walker 1 and (-1)1(-1)

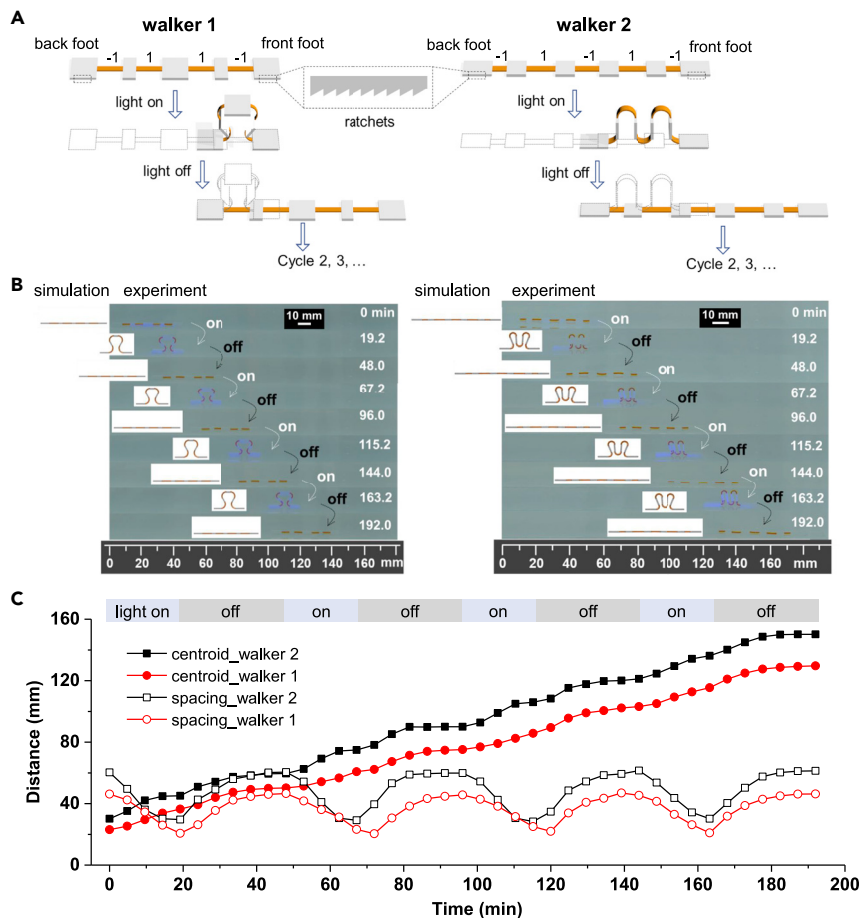


Figure 4. Unidirectional inchworm-like crawling motion of linear macroscopic constructs

(A) Schematic representation of light-triggered unidirectional inchworm-like locomotion achieved by linear hydrogel walkers; left, an object with code of $(-1)11(-1)$; right, an object with code of $(-1)1(-1)1(-1)$, and ratcheted structures were built on the bottom surface of front and back feet highlighted with dashed rectangles.

(B) Photographs of four walking cycles of each hydrogel walker by controlling the light irradiation on or off (the time at which each photograph was taken is indicated in the upper right-hand corner); left, an object with code of $(-1)11(-1)$; right, an object with code of $(-1)1(-1)1(-1)$; snapshots from finite element simulations are shown on the left side of photographs from experiments.

(C) Plot of the spacing between front and back feet and the displacement of the centroid of the hydrogel walkers versus time by switching the light on and off for four walking cycles.

$1(-1)$ for walker 2) whose front and back feet are functionalized with the ratchets. Due to anisotropic friction with the substrate, the front foot stands still while the back foot moves forward during the photo-induced bending process. Conversely, the front foot moves forward while the back foot stands still during the flattening process once the light is off. Consequently, the walkers move forward unidirectionally for one single step. By alternately switching the light on and off, multi-step unidirectional locomotion from left to right was achieved, in good agreement with the results from finite element simulations (Figure 4B; Video S6). The spacing between front and back feet changed alternately along with the light being switched on and off, and the centroid of the object moved forward smoothly over a macroscopic distance over four walking cycles (107 mm for walker 1; 120 mm for walker 2, Figure 4C), indicating the high reversibility and robustness of the systems. In contrast to previously reported actuators that can only walk on specific substrates containing special

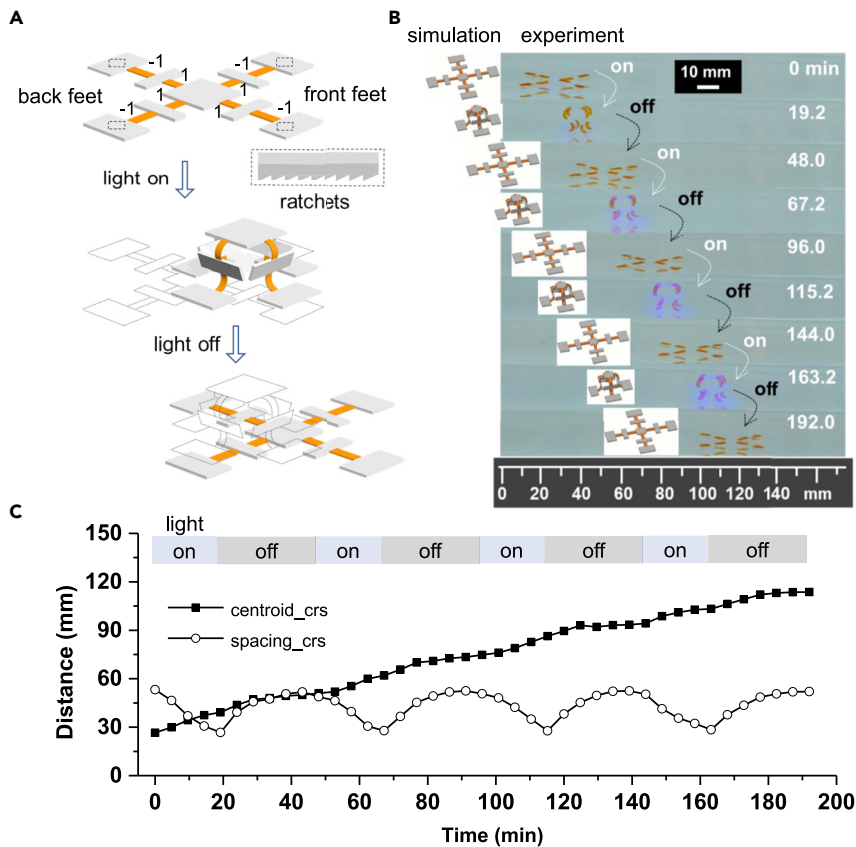


Figure 5. Unidirectional octopus-like walking motion of cross-shaped macroscopic construct
 (A) Schematic representation of light-triggered unidirectional octopus-like locomotion achieved by a cross-shaped hydrogel walker; ratcheted structures were built on the bottom surface of front and back feet highlighted with dashed rectangles.
 (B) Photographs of four walking cycles of the cross-shaped hydrogel walker achieved by controlling whether or not light irradiation was on or off (left, snapshots from finite element simulations; right, photographs from experiments). The time at which each photograph was taken is indicated in the upper right-hand corner.
 (C) Plot of the spacing between front and back feet and the displacement of the centroid of the cross-shaped hydrogel walker versus time by switching the light on and off for four walking cycles.

features, the direction of this inchworm-like motion is determined by the built-in ratchets and does not rely on the features or roughness of the substrate.

Octopus-like walking motion of cross-shaped macroscopic construct

To expand locomotion gait, we developed a cross-shaped hydrogel walker with four feet containing built-in ratcheted patterns and obtained motion similar to that of an octopus. The ratchets were aligned perpendicular to the walking axis to obtain better control of unidirectional movement. Figure 5A illustrates the walking mechanism based on the bending–flattening process by switching the light on and off. Unlike the inchworm-like movement discussed previously, the front feet collapsed in the direction perpendicular to the walking motion instead of completely standing still during the bending process under irradiation. Also, the back feet relaxed in the direction perpendicular to the walking motion while the front feet moved forward during the flattening process in the dark. Consequently, a unidirectional octopus-like motion was achieved, which could be repeated and cycled multiple times by switching the light on and off (Figure 5B) to achieve macroscopic locomotion (Figure 5C;

[Video S7](#)). This octopus-like walking behavior was also investigated by finite element simulations (see the [Experimental procedures](#) for details).

Conclusions

We have designed and synthesized photoactive bilayer hydrogel actuators that respond to a single stimulus of light through the synergistic effect of photoexpansion and photocontraction. The synergistic photoactuator displayed a larger deformation gradient between the two layers and a faster reversible bending/relaxing speed relative to conventional actuators in which only one layer is photoresponsive. Encoding these bilayers into linear, cross-shaped, and branched hydrogel structures with a pre-determined sequence, enabled highly programmed shape transformations upon light irradiation. By incorporating anisotropic ratcheted patterns into their bodies, these hydrogel objects exhibited improved motions over macroscopic distances by alternately switching the light source on and off, and the walking motions were independent of the substrate features. Importantly, all these shape changes and the locomotion observed in experiments were predicted by finite element simulations. We anticipate that the biomimetic strategy to create synergistic bilayer photoactuators demonstrated here will benefit the design and development of other functional soft materials that mimic or surpass the functions observed in living organisms. Furthermore, the use of such bilayer hydrogels could enable their application as responsive biomaterials and could be designed to involve stimuli other than light.

EXPERIMENTAL PROCEDURES

Resource availability

Lead contact

Further information and requests for resources and reagents should be directed to and will be fulfilled by the lead contact, Samuel I. Stupp (s-stupp@northwestern.edu).

Materials availability

This study did not generate new unique reagents. Chemicals used for synthesis of spiropyran molecules and chemicals used for hydrogel preparation (*N*-isopropylacrylamide, *N,N'*-methylenebisacrylamide, ammonium persulfate, etc.) were purchased from Sigma-Aldrich, Thermo Fisher Scientific, or other commercial companies, and used directly without any purification unless mentioned. The UV-curable resin was purchased from Loon Outdoors (UV Clear Fly Finish Thick). The plain glass slides (75 × 38 × 1.0 mm) used for making molds were purchased from Thermo Fisher Scientific. The plastic spacer (300 μm thick) was purchased from Amazon. The blue LED (450 nm) was purchased from Luxeon Star LEDs. The UV lamp (Analytik Jena UVL-21 UV Lamp, 4-W, 365 nm) was purchased from Cole Parmer. The power and energy meter was purchased from Thorlabs (Digital Handheld Optical Power and Energy Meter Console, Model PM100D). Videos and photographs of photoactuation and locomotion experiments were taken using a Nikon D5600 DSLR camera with a macro lens (Sigma 105 mm f/2.8 EX DG OS HSM Macro).

Data and code availability

All data needed to evaluate the conclusions in the paper are present in the paper and/or the [Supplemental information](#). Additional data related to this study are available from the corresponding authors upon reasonable request.

Bilayer hydrogel preparation

Spiropyran was first synthesized following our previously reported procedure⁴⁶ ([Scheme S1](#), see the [Supplemental information](#) for details). Bilayer hydrogels were

prepared through a sequential layer-by-layer polymerization process within glass molds as described in [Scheme S2](#). The thickness of each layer is controlled by the thickness of plastic spacers adhered to the glass slides using a UV-curable resin. The first layer is only partially polymerized to form a soft gel followed by immediately adding and polymerizing the second layer to ensure the creation of chemical linking between two layers. The polymerization solution (1 mL) is prepared in water (for photoexpanding and blank layer) or a dioxane/water mixture (v/v, 4:1, for photocontracting layer) by adding *N*-isopropylacrylamide monomer (10 wt%, 100 mg), *N,N'*-methylenebisacrylamide crosslinker (0.68 wt%, 6.8 mg), and spiropyran molecule (1.0 wt%, 10 mg). This solution is cooled down to 4°C. To initialize the polymerization, ammonium persulfate (10 wt%, 50 μL) and *N,N,N',N'*-tetramethylethylenediamine (3.7 μL) were added to the polymerization solution (1 mL) and vigorously vortexed before pipetting into glass molds. After being partially polymerized at 4°C, a soft gel formed, and the top glass slide was gently opened and the second spacers were added, followed by re-sealing the glass molds using a UV-curable resin. The second polymerization solution was freshly initiated and immediately added to the re-sealed glass mold and totally polymerized. After de-molding, the bilayer gels were exchanged to methanol for 10 min to wash out excess unreacted monomer and initiator, then exchanged to 5 mM aqueous HCl for 2 h in the dark before the actuation experiments. Bilayer hydrogels were cut to the desired shape using a razor blade. Blank layers were prepared following the same protocol but without the presence of spiropyran molecules. Photoexpanding hydrogels containing polyacrylamide (10 wt%) were prepared in water and photocontracting hydrogels containing polyacrylamide (10 wt%) were prepared in a dimethyl sulfoxide/water mixture (v/v, 4:1) following the same formulation and protocol.

Photoactuation study

Hydrogel samples were first placed in acidic water containing 5 mM HCl to protonate the merocyanine form, then transferred to a large tank of Milli-Q water. Photoactuation was immediately started by irradiating blue light (450 nm, 78 mW/cm²) on the hydrogel samples. The light source we used was a blue LED (Ustellar, 30 W, IP66) that contains a 4 × 7 array of LEDs. The size of the light spot is 60 × 25 mm, which is slightly larger than all the actuators, to effectively guarantee that the actuators are uniformly irradiated. Light intensity was adjusted by changing the distance between the light spot and the actuator. The volume ratio of single-layer samples was calculated based on the area change of the samples. The bending angles or bending speed of bilayer hydrogel samples was calculated by measuring the angles of each photograph/frame using ImageJ software (<https://imagej.net/Citing>). After photoactuation, the hydrogel samples were transferred to another tank of acidic water (5 mM HCl) to recover to their original state, which could be used for the second photoactuation process. This recovery process in the dark was also tracked by taking photographs using the same camera. The maximum bending angle of bilayer hydrogel samples was obtained by irradiating the samples until their bending angles no longer changed. The photoactuation of block structures, including linear, cruciform, and branched objects, as well as hydrogel walkers, were also carried out following the same protocol described above. All these samples were protonated in acidic water (5 mM HCl) first and then transferred to neutral Milli-Q water for photoactuation studies. Samples were allowed to relax in acidic water (5 mM HCl) in the dark. For each walking step of the actuator, the light source was moved forward to match the walker's position to ensure that the light always uniformly covered the whole actuator.

Preparation of programmed block structures

The block structures described in [Figure 3](#) were prepared by chemically bonding photoinactive components and photoactive bilayer components followed by a

manual cutting process. First, the synergistic bilayer was cut into small uniform bridge units (dimensions: 6 mm long, 2 mm wide, and 0.3 + 0.3 mm thick), and *con-exp* was named +1 while the opposite *exp-con* was named -1. Second, these bridge units were placed at the desired locations on a glass slide with predetermined sequence of +1 and -1 according to the linear pattern. Spacers (0.55 mm thick) and another glass slide were added on top and sealed using UV-cured glue to obtain a glass mold. The thickness of spacers used here is slightly thinner than the thickness of bilayer hydrogels so that these bridge units are squeezed and fixed at the desired positions by the two glass sides. Third, a monomer solution containing NIPAM, MBAAm, and APS/TEMED, but without spiropyrans, was gently added to this glass mold, followed by a free radical polymerization which covalently connected and fixed the bridge units inside the mold. After carefully de-molding, the photoinactive component was manually cut into squares or rectangles according to the pattern, giving the final linear block structures. Other linear block structures were prepared following the same protocol described above but with different permutations of the four photoactive units during the preparation process, with each individual unit being either 1 or -1. Cross-shaped or branched structures were prepared following the same protocol described for the linear structures using a corresponding cross-shaped or branched pattern.

Preparation of hydrogel walkers with built-in ratcheted patterns

To build ratcheted structures into the hydrogel bodies, we first printed a plastic mold containing the ratcheted patterns using a 3D printer. The dimensions of these ratchets are 0.25 mm high by 0.35 mm wide (Scheme S3). After assembling spacers with desired thickness, a monomer solution containing a NIPAM monomer, a MBAAm crosslinker, and an APS/TEMED initiator was added on top of the plastic mold, and then covered by a smooth plastic slide. After polymerization, the top mold was carefully opened, and the hydrogel was gently peeled off from the mold. Hydrogels containing ratcheted patterns were further cut into small building blocks, named ratcheted units, with the following dimensions: 10 mm long, 6 mm wide, and 0.6 mm thick. With ratcheted units and photoactive bridge units in hand, we followed the same protocol described above to prepare the block structures. As an example of linear block structure (Scheme S3b), ratcheted units (purple) and bridge units (orange) were both placed at the desired locations according the linear pattern, followed by addition of a solution containing the monomers/cross-linkers/initiators to form blank hydrogels that could covalently connect and fix these building blocks. After de-molding and cutting, linear block structures with both photoactive bridge units and ratcheted units were obtained. The cross-shaped block structures were prepared following the same protocol.

Analytical modeling

An analytical model was developed to predict the bending curvature of bilayer photoactuators. Here, we let L_0 denote the initial length of flat bilayer photoactuators (for both top and bottom layers). After exposure to light, the top/bottom layers may expand, contract, or remain undeformed, depending on the types of photoresponsive materials used (denoted by *exp*, *con*, or *bl*, respectively). The new stress-free lengths for top and bottom layer after light exposure then become

$$\begin{aligned} L_1 &= L_0 \lambda_1, \\ L_2 &= L_0 \lambda_2, \end{aligned} \quad \text{Equation S1}$$

where λ_1 and λ_2 are the deformation ratios of top and bottom layers. The mismatch of the deformation in the top and bottom layers lead to bending of the bilayers with an arc angle α , and bending radius R_0 at the interface of the bonded top/bottom

layers, where α and R_0 are to be determined. At position y along the thickness direction ($y = 0$ is at the bonding interface), the axial normal stresses σ_1 and σ_2 are given by

$$\begin{aligned}\sigma_1 &= E_1 \left(\frac{R_0 \alpha + y \alpha}{L_1} - 1 \right), \\ \sigma_2 &= E_2 \left(\frac{R_0 \alpha + y \alpha}{L_2} - 1 \right).\end{aligned}\tag{Equation S2}$$

where E_1 and E_2 are moduli of the top and bottom layers, respectively. Mechanical equilibrium requires the net forces and moments to be zero, yielding

$$\begin{aligned}\int_0^{t_1} \sigma_1 dy + \int_{-t_2}^0 \sigma_2 dy &= 0, \\ \int_0^{t_1} \sigma_1 y dy + \int_{-t_2}^0 \sigma_2 y dy &= 0,\end{aligned}\tag{Equation S3}$$

where t_1 and t_2 are thicknesses of the top and bottom layers, respectively. Combining Equations S1, S2, and S3, the arc angle can be determined as

$$\alpha = \frac{L_0}{t_1} \frac{6\eta(1+\eta)\lambda_1\lambda_2(\lambda_1 - \lambda_2)\xi}{\eta^4\lambda_1^2\xi^2 + (4\eta + 6\eta^2 + 4\eta^3)\lambda_1\lambda_2\xi + \lambda_2^2},\tag{Equation S4}$$

where $\eta = t_2/t_1$, and $\xi = E_2/E_1$. Please note the arc angle α is four times the bending angle in main text.

The material properties, including mechanical modulus and deformation ratio used for Figure 2, are listed in Table S1.

Bending moment calculation

The initially flat bilayer photoactuators form a curved shape due to expanding/contraction of top/bottom layers upon exposure to light. The generated actuation force can be quantified by the bending moment that is required to flatten back the bent bilayer. The analytical model developed above can be easily extended to include an external bending moment by revising Equation S3 as

$$\begin{aligned}\int_0^{t_1} \sigma_1 dy + \int_{-t_2}^0 \sigma_2 dy &= 0, \\ \int_0^{t_1} \sigma_1 y dy + \int_{-t_2}^0 \sigma_2 y dy &= -\frac{M}{W},\end{aligned}\tag{Equation S5}$$

where M is the applied external bending moment and W is the width. By enforcing the arc angle α to be zero, we solve the bending moment required to flatten the bilayer system as

$$M = W \frac{E_1 t_1^2 \eta \xi (1 + \eta) (\lambda_1 - \lambda_2)}{2(\lambda_2 + \lambda_1 \eta \xi)}.\tag{Equation S6}$$

Finite element analysis

3D finite element analysis (FEA) was used to study the shape evolution of the bilayer structures. Eight-node 3D solid elements (Abaqus element type C3D8R) were used for the whole system. Expansion or contraction is applied to top/bottom layers depending on their response to light. The deformation ratios applied in FEA for obtaining structures shown in Figure 3 match well with the experimental ratios, which are listed in Table S2.

SUPPLEMENTAL INFORMATION

Supplemental information can be found online at <https://doi.org/10.1016/j.matt.2021.01.016>.

ACKNOWLEDGMENTS

This work was fully supported by the Center for Bio-Inspired Energy Science (CBES), an Energy Frontier Research Center funded by the U.S. Department of Energy (DOE), Office of Science, Basic Energy Sciences under award no. DE-SC0000989. This work made use of the IMSERC at Northwestern University, which has received support from the NIH (1S10OD012016-01/1S10RR019071-01A1), Soft and Hybrid Nanotechnology Experimental (SHyNE) Resource (NSF ECCS-1542205), the State of Illinois, and the International Institute for Nanotechnology (IIN). This work made use of the MatCI Facility, which receives support from the MRSEC program (NSF DMR-1720139) of the Materials Research Center at Northwestern University. This work made use of the EPIC facility of Northwestern University's NUANCE Center, which has received support from SHyNE Resource (NSF ECCS-1542205); the MRSEC program (NSF DMR-1720139) at the Materials Research Center; the IIN; the Keck Foundation; and the State of Illinois, through the IIN. We thank Nicholas A. Sather for helpful discussion and Mark Seniw for providing schematic illustrations.

AUTHOR CONTRIBUTIONS

C.L. designed and conducted the experiments and wrote the initial draft of the manuscript. Y.X. performed the analytical model and finite element simulations. M.H. helped with the design of the ratcheted patterns. L.C.P., J.A.R., Y.H., and S.I.S. supervised the research and wrote the manuscript.

DECLARATION OF INTERESTS

The authors declare no conflict of interest.

Received: October 22, 2020

Revised: December 28, 2020

Accepted: January 13, 2021

Published: February 9, 2021

REFERENCES

- Dawson, C., Vincent, J.F.V., and Rocca, A.M. (1997). How pine cones open. *Nature* 390, 668.
- Elbaum, R., Zaltzman, L., Burgert, I., and Fratzl, P. (2007). The role of wheat awns in the seed dispersal unit. *Science* 316, 884–886.
- Harrington, M.J., Razghandi, K., Ditsch, F., Guiducci, L., Rueggeberg, M., Dunlop, J.W.C., Fratzl, P., Neinhuis, C., and Burgert, I. (2011). Origami-like unfolding of hydro-actuated ice plant seed capsules. *Nat. Commun.* 2, 337.
- Tada, A., Geng, Y.F., Wei, Q.S., Hashimoto, K., and Tajima, K. (2011). Tailoring organic heterojunction interfaces in bilayer polymer photovoltaic devices. *Nat. Mater.* 10, 450–455.
- Kharlampieva, E., Kozlovskaya, V., and Sukhishvili, S.A. (2009). Layer-by-layer hydrogen-bonded polymer films: from fundamentals to applications. *Adv. Mater.* 21, 3053–3065.
- Khan, M.K., Hamad, W.Y., and MacLachlan, M.J. (2014). Tunable mesoporous bilayer photonic resins with chiral nematic structures and actuator properties. *Adv. Mater.* 26, 2323–2328.
- Wang, S., Gao, Y., Wei, A., Xiao, P., Liang, Y., and Lu, W.; Chen C., Zhang C., Yang G., Yao H., Chen T (2020). Asymmetric elastoplasticity of stacked graphene assembly actualizes programmable untethered soft robotics. *Nat. Commun.* 11, 4359.
- Liu, S., Yao, Z., Chiou, K., Stupp, S.I., and Olvera de la Cruz, M. (2016). Emergent perversions in the buckling of heterogeneous elastic strips. *Proc. Natl. Acad. Sci. USA* 113, 7100–7105.
- Boothby, J.M., and Ware, T.H. (2017). Dual-responsive, shape-switching bilayers enabled by liquid crystal elastomers. *Soft Matter* 13, 4349–4356.
- Agrawal, A., Yun, T.H., Pesek, S.L., Chapman, W.G., and Verduzco, R. (2014). Shape-responsive liquid crystal elastomer bilayers. *Soft Matter* 10, 1411–1415.
- Le, X., Lu, W., Zhang, J., and Chen, T. (2019). Recent progress in biomimetic anisotropic hydrogel actuators. *Adv. Sci.* 6, 1801584.
- Liu, G., Ding, Z., Yuan, Q., Xie, H., and Gu, Z. (2018). Multi-layered hydrogels for biomedical applications. *Front. Chem.* 6, 439.
- He, X., Zhang, D., Wu, J., Wang, Y., Chen, F., and Fan, P.; Zhong M., Xiao S., Yang J (2019). One-pot and one-step fabrication of salt-responsive bilayer hydrogels with 2D and 3D shape transformations. *Acs Appl. Mater. Interfaces* 11, 25417–25426.
- Hu, Z., Zhang, X., and Li, Y. (1995). Synthesis and application of modulated polymer gels. *Science* 269, 525–527.
- Ionov, L. (2014). Hydrogel-based actuators: possibilities and limitations. *Mater. Today* 17, 494–503.

16. Erol, O., Pantula, A., Liu, W., and Gracias, D.H. (2019). Transformer hydrogels: a review. *Adv. Mater. Technol.* **4**, 1900043.
17. Gladman, A.S., Matsumoto, E.A., Nuzzo, R.G., Mahadevan, L., and Lewis, J.A. (2016). Biomimetic 4D printing. *Nat. Mater.* **15**, 413–418.
18. Cangialosi, A., Yoon, C., Liu, J., Huang, Q., Guo, J., and Nguyen, T.D.; Gracias D.H., Schulman R (2017). DNA sequence-directed shape change of photopatterned hydrogels via high-degree swelling. *Science* **357**, 1126–1129.
19. Cheng, Y., Ren, K., Yang, D., and Wei, J. (2018). Bilayer-type fluorescence hydrogels with intelligent response serve as temperature/pH driven soft actuators. *Sensor Actuat. B-Chem.* **255**, 3117–3126.
20. Zhang, Z.H., Chen, Z., Wang, Y., Chi, J., Wang, Y., and Zhao, Y. (2019). Bioinspired bilayer structural color hydrogel actuator with multienvironment responsiveness and survivability. *Small Methods* **3**, 1900519.
21. Li, X., Cai, X., Gao, Y., and Serpe, M.J. (2017). Reversible bidirectional bending of hydrogel-based bilayer actuators. *J. Mater. Chem. B* **5**, 2804–2812.
22. Li, J., Ma, Q., Xu, Y., Yang, M., Wu, Q., and Wang, F.; Sun P (2020). Highly bidirectional bendable actuator engineered by LCST-UCST bilayer hydrogel with enhanced interface. *ACS Appl. Mater. Interfaces* **12**, 55290–55298.
23. Li, Q., Schenning, A.P.H.J., and Bunning, T.J. (2019). Light-responsive smart soft matter technologies. *Adv. Opt. Mater.* **7**, 1901160.
24. Bertrand, O., and Gohy, J.F. (2017). Photo-responsive polymers: synthesis and applications. *Polym. Chem.* **8**, 52–73.
25. Gelebart, A.H., Mulder, D.J., Varga, M., Konya, A., Vantomme, G., and Meijer, E.W.; Selinger R.L.B., Broer D.J (2017). Making waves in a photoactive polymer film. *Nature* **546**, 632–636.
26. Hu, Y., Li, Z., Lan, T., and Chen, W. (2016). Photoactuators for direct optical-to-mechanical energy conversion: from nanocomponent assembly to macroscopic deformation. *Adv. Mater.* **28**, 10548–10556.
27. Ruskowitz, E.R., and DeForest, C.A. (2018). Photoresponsive biomaterials for targeted drug delivery and 4D cell culture. *Nat. Rev. Mater.* **3**, 17087.
28. Cheng, Y.C., Lu, H.C., Lee, X., Zeng, H., and Priimagi, A. (2020). Kirigami-based light-induced shape-morphing and locomotion. *Adv. Mater.* **32**, 1906233.
29. Li, L., Scheiger, J.M., and Levkin, P.A. (2019). Design and applications of photoresponsive hydrogels. *Adv. Mater.* **31**, 1807333.
30. Takashima, Y., Hatanaka, S., Otsubo, M., Nakahata, M., Kakuta, T., and Hashidzume, A.; Yamaguchi H., Harada A (2012). Expansion-contraction of photoresponsive artificial muscle regulated by host-guest interactions. *Nat. Commun.* **3**, 1270.
31. Lee, T.T., Garcia, J.R., Paez, J.I., Singh, A., Phelps, E.A., and Weis, S.; Shafiq Z., Shekaran A., del Campo A., Garcia A.J (2015). Light-triggered in vivo activation of adhesive peptides regulates cell adhesion, inflammation and vascularization of biomaterials. *Nat. Mater.* **14**, 352–360.
32. Ouyang, L.L., Highley, C.B., Sun, W., and Burdick, J.A. (2017). A generalizable strategy for the 3D bioprinting of hydrogels from nonviscous photo-crosslinkable inks. *Adv. Mater.* **29**, 1604983.
33. Russev, M.M., and Hecht, S. (2010). Photoswitches: from molecules to materials. *Adv. Mater.* **22**, 3348–3360.
34. Pianowski, Z.L. (2019). Recent implementations of molecular photoswitches into smart materials and biological systems. *Chem. Eur. J.* **25**, 5128–5144.
35. Mogaki, R., Okuro, K., and Aida, T. (2017). Adhesive photoswitch: selective photochemical modulation of enzymes under physiological conditions. *J. Am. Chem. Soc.* **139**, 10072–10078.
36. Chen, J., Leung, F.K.-C., Stuart, M.C.A., Kajitani, T., Fukushima, T., and van der Giessen, E.; Feringa B.L (2018). Artificial muscle-like function from hierarchical supramolecular assembly of photoresponsive molecular motors. *Nat. Chem.* **10**, 132–138.
37. Li, C., Iscen, A., Sai, H., Sato, K., Sather, N.A., and Chin, S.M.; Alvarez Z., Palmer L.C., Schatz G.C., Stupp S.I (2020). Supramolecular-covalent hybrid polymers for light-activated mechanical actuation. *Nat. Mater.* **19**, 900–909.
38. Foy, J.T., Li, Q., Goujon, A., Colard-Itté, J.-R., Fuks, G., and Moulin, E.; Schiffmann O., Dattler D., Funeriu D.P., Giuseppone N (2017). Dual-light control of nanomachines that integrate motor and modulator subunits. *Nat. Nanotech.* **12**, 540–545.
39. Lancia, F., Ryabchun, A., and Katsonis, N. (2019). Life-like motion driven by artificial molecular machines. *Nat. Rev. Chem.* **3**, 536–551.
40. Kortekaas, L., and Browne, W.R. (2019). The evolution of spiropyran: fundamentals and progress of an extraordinarily versatile photochrom. *Chem. Soc. Rev.* **48**, 3406–3424.
41. Klajn, R. (2014). Spiropyran-based dynamic materials. *Chem. Soc. Rev.* **43**, 148–184.
42. Sumaru, K., Ohi, K., Takagi, T., Kanamori, T., and Shinbo, T. (2006). Photoresponsive properties of poly(*N*-isopropylacrylamide) hydrogel partly modified with spiropyrans. *Langmuir* **22**, 4353–4356.
43. Francis, W., Dunne, A., Delaney, C., Florea, L., and Diamond, D. (2017). Spiropyran based hydrogels actuators—walking in the light. *Sensor Actuat. B Chem.* **250**, 608–616.
44. Satoh, T., Sumaru, K., Takagi, T., and Kanamori, T. (2011). Fast-reversible light-driven hydrogels consisting of spiropyrans-functionalized poly(*N*-isopropylacrylamide). *Soft Matter* **7**, 8030–8034.
45. Li, C., Lau, G.C., Yuan, H., Aggarwal, A., Dominguez, V.L., and Liu, S.; Sai H., Palmer L.C., Sather N.A., Pearson T.J., et al (2020). Fast and programmable locomotion of hydrogel-metal hybrids under light and magnetic fields. *Sci. Robot.* **6**, eabb9822.
46. Li, C., Iscen, A., Palmer, L.C., Schatz, G.C., and Stupp, S.I. (2020). Light-driven expansion of spiropyran hydrogels. *J. Am. Chem. Soc.* **142**, 8447–8453.